Science Arena Publications
Specialty Journal of Electronic and Computer Sciences
ISSN: 2412-7485
Available online at www.sciarena.com
2018, Vol, 4 (4):16-30

Designing of Sliding Mode Controller for Active and Reactive Power for Generator Connected to Network

Mohammad Hossein Atazadeghan

M.Sc in Electrical Engineering (Power), Islamic Azad University, Jahrom Branch, Iran.

Abstract: *Doubly-Fed Induction Generators (DFIG) have recently attracted the attention of many users, and have also caused an increase in the demands, due to their special features and unique advantages. When this type of generator is in an unbalanced network, the voltage unbalance may lead to the disruptions in the generator's function that can involve the generation of pulses in the, active, and reactive powers and electromagnetic torque, unbalance in the stator's current, and finally, harmonization of the rotor's current. One of the most remarkable approaches in designing a resistant controller is the sliding mode control. Clearly, controlling a system expressed by a first order differential equation is much simpler than controlling a system expressed by nth order differential equation. This feature is used in the sliding mode control, and using a conversion (sliding surface), it is shown that it can be possible to obtain a resistant control. In this research, the simulation of the suggested control strategy for DFIG-based wind power generation system is done by using MATLAB software. The most significant innovations that are realized by the current research are increasing the efficiency, optimizing the power coefficient, and increasing the quality and controlling maneuver by the sliding mode.*

Keywords: *Sliding Mode Control, Active and Reactive Power Control of the Induction Generator, Grid-Connected Doubly-Fed Generator.*

INTRODUCTION

The properties of a doubly-fed induction generator include a wound rotor induction machine that its stator is directly connected to the grid and rotor windings are connected to the grid by means of a back-to-back converter. There are lots of approaches for the optimal control of this generator to achieve efficient performance in balanced networks. Sliding mode control, PI classical control, direct torque control, and direct power control are among the aforementioned approaches. If this type of generator is put in an unbalanced network, the voltage unbalance may lead to the disruptions in the generator's function that can involve the generation of pulses in the active, and reactive powers, and electromagnetic torque, unbalance in the stator's current, and finally, harmonization of the rotor's current (Hu et al., 2010)

There are many problems with the application of designed controllers to real systems. One of the most important roots of these problems is the inability to model the real systems accurately (Bartolini et al., 2003). Furthermore, even if the ability for this accurate modelling exists, the resulting model would be so complicated that it makes designing an appropriate controller difficult. Resistant control, and comparative control, are two remarkable and supplementary methods for overcoming the above-mentioned problem. There are two elements in the structure of a resistant controller: the aim of one is to control the system (such as revers-acting control, and linearized control), and the aim of the other is to handle the inaccuracies in the model. The structure of a comparative controller – which is a type of resistant controller – is similar, except

that in a comparative controller the model is continuously updated based on the obtained information (Shtessel et al., 2014)

One of the most prominent approaches in designing a resistant controller is the sliding mode control. This property is used in the sliding mode control, and using a conversion (sliding surface) it is shown that it can be possible to obtain a resistant control. Sliding mode control is able to accomplish active and reactive power control of the converter, preserve the nonlinear properties of the converter and the power, and perform well against the disturbances and other errors.

In (Bekka et al., 2013) designing a controller, and investigating its performance in controlling wind turbines in strong winds condition is addressed. In (Bianchi et al., 2010) classical control methods are used, and in (Bektacheand Boukhezzar, 2018; Boukhezzar et al., 2007) the comparative LQG control method is used. In (Ramadgeand Wonham, 1987) a monitoring control method is used for wind turbines. In (Yu, 2017; Rocha-Osorio et al., 2018) designing a remote controller for turbines is studied. In the above article, morphologic filtering is used to achieve the desirable power quality. Furthermore, the method has attempted at eliminating the unwanted harmonics, and optimizing the system's response. Finally, the structural control of (Zuo et al., 2018) is another controlling method that is applied on wind turbine systems. In the above paper, namely (Zuo et al., 2018), the wind turbine is studied as a mathematical model based on Euler-Lagrange method.

In order to reduce the undesirable impacts of voltage unbalance in the generator, this paper employs the sliding mode control method. Due to the fact that reactive power is one the most significant factors in designing and utilizing AC electric power systems, in this method designing and utilizing a control system is done to achieve the aims of eliminating electromagnetic torque, balancing the stator's current, eliminating the harmonics from the rotor's current, and eliminating the pulses in active and reactive powers.

In the second section that follows DFIG is studied, and modelling of the wind turbine on its basis is addressed. In the third section, sliding mode control method is studied in detail. The fourth section is related to the proposed control method and also the simulation.

What is sliding mode or SMC? It is an eminent control method based on using a discontinuous control input. The importance of this method lies in its resistance against a certain class of uncertainties that affect the system. SMC causes a controlled system to evolve as a variable structure system, and leads the system's condition, in a finite and limited time, to a predetermined level that is technically called the sliding surface. Therefore, since the time is limited, sliding mode occurs (Wu et al., 2018).

The characteristics of SMC are:

1. Adequate controlling performance in tracking mode even for nonlinear systems
2. Applicability to systems that vary with time
3. Resistance to uncertainties
4. Simplicity of application on multiple input and output systems (Shtessel et al., 2014)

The Model of Wind Turbine System with DFIG

The Structure of a Wind Power Plant

Before addressing the issues related to the compatibility of a wind turbine and a doubly-fed induction generator, and also their connection, shown in Figure 1 (Sitharthan et al., 2018), it is necessary to provide a brief explanation of wind turbines.

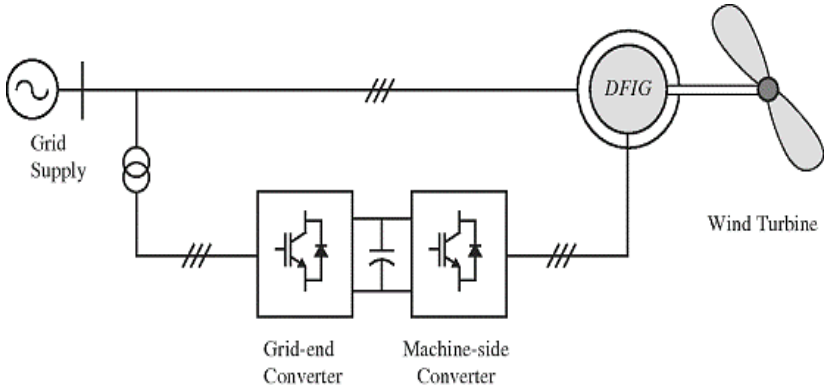

Figure 1. Connection of the wind turbine to the grid and DFIG (Sitharthan et al., 2018)

The wind power plant is designed in such a way that the DFIG's stator circuit is directly connected to the grid, while the rotor circuit is connected by means of a back-to-back converter with sliding loops. A capacitor, called DC link, is put between the two converters. This capacitor acts as an energy storage device, and is used to keep the voltage sTable. In usual performance conditions, DFIG can separately control the active and reactive power that is needed in the system (Yanhua et al., 2011). This is done through a control method known as monocycle control (Femia et al., 2009; Duon et al., 2018). In this paper, the proposed method is applied on a doubly-fed generator.

The Model of a Wind Turbine

The equations of a wind turbine are as follows:

$$P_m(u) = \frac{1}{2} C_P(\lambda, \beta) \rho \pi R^2 u^3 \quad (1)$$

$$\lambda = \frac{R\omega_{rot}}{u} \quad (2)$$

$$C_Q = {}^{C_P}/_{\lambda} \quad (3)$$

In which ρ is the density of air, R is the radius of the rotor, and u is the wind's speed. Furthermore, $C_p$is the turbine's generation coefficient that is, in fact, the ratio of output power to wind power. The maximum obtainable value for this coefficient is called Betz limit which is equal to $C_{P_{Max}} = \frac{16}{27} = 0.593$. This maximum limit is employed in any type of wind turbine. The power coefficient is usually provided by the manufacturers. $\lambda$is also the ratio of tip speed to edge speed, in which $\omega_{rot}$is the rotor's angular speed.

$C_Q$is the torque coefficient. In case of a fixed-pitch wind turbine, coefficients $C_p$and $C_Q$vary with λ only, and it is considered that $\beta = 0$.

The Model of DFIG Generator

Due to the lack of synchronicity between the rotor and stator of induction generators and machines, they are called asynchronous (Munje et al., 2018). Therefore, similar to an induction motor, an induction generator functions in sub-synchronous and super-synchronous speeds. The following equations express this issue:

(4)

$$V_s^s = R_s I_s^s + \frac{d\varphi_s^s}{dt} + j\omega_s \varphi_s^s$$

$$V_r^s = R_r I_r^s + \frac{d\varphi_r^s}{dt} + j(\omega_s - \omega_r)\varphi_r^s$$

$$\varphi_s^s = L_s I_s^s + L_m I_r^s$$

$$\varphi_r^s = L_m I_s^s + L_r I_r^s$$

In the above equation, $L_s = L_{\delta s} + L_m$ and $L_r = L_{\delta r} + L_m$.

Modelling a Wind Turbine Based on DFIG

DFIG-based wind turbine system shown in fig. 2 is made up of the following components: aerodynamic subsystem, DFIG subsystem, and the propulsion subsystem (powertrain). The fact that one of the main strategies is planned based on two circles can be inferred from fig. 2: the internal circle that adjusts the rotor's current (torque), and the external circle that is used for tracking the power point.

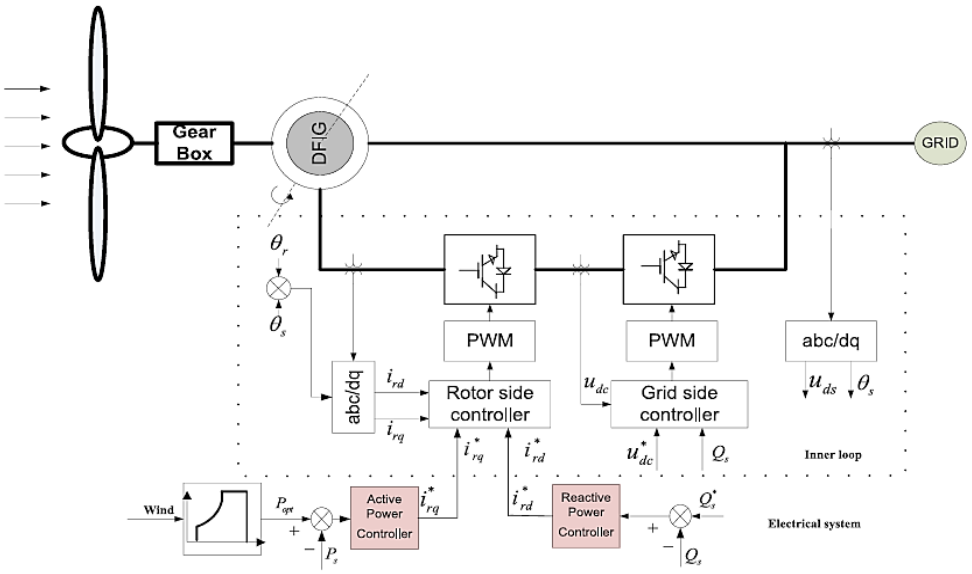

Figure 2. DFIG wind turbine system (Hu et al., 2010)

The approximate values for the aerodynamic force P_a and torque $T_a$are obtained through the following equation.

(5)

$$\begin{cases} P_a = \frac{1}{2}\rho\pi R2\, v3\, Cp(\lambda, \beta) \\ Tp = \frac{1}{2}\rho\pi R2\, v3\, Cp(\lambda, \beta)/\lambda \end{cases}$$

In which λ is the ratio of tip speed and we have $\lambda = \omega_m R/v$. R is the blade's radius, v is the wind speed, ρ is the air density, isthe pitch angle, $C_p$is the power coefficient, and $\omega_m$is the rotor speed. The relations related to the induction generator can be written in dq desired form as follows:

(6)

$$\begin{cases} u_{sd} = R_s i_{sd} - \omega_s i_{sd} + \dot{\psi}_{sd} \\ u_{sq} = R_s i_{sq} + \omega_s i_{sq} + \dot{\psi}_{sq} \\ u_{rd} = R_s i_{rd} - \omega_r i_{rd} + \dot{\psi}_{rd} \\ u_{rq} = R_s i_{rq} + \omega_s i_{rq} + \dot{\psi}_{rq} \end{cases}$$

In DFIG subsystem, the aerodynamic torque is transferred to the generator part by means of a gearbox. The propulsion subsystem can be simplified regardless of the losses due to friction. It can be expressed as:

(7)

$$T_a\_T_e = J\omega_m + B\omega_m$$

In which T_a is equal to the aerodynamic torque, J is equal to the moment of inertia, B is the damping coefficient, and $T_e$is the magnetic torque.

|DFIG Control Strategy Applied on a Wind Turbine

Models equal to the rotor dynamics can be achieved through:

(8)

$$\begin{cases} i_{rd} = -(R_r i_{rd\_} \omega_r i_{rq})/\delta L_r + u_{rd}/\delta L_r \\ i_{rq} = -\dfrac{R_r i_{rq} + \omega_r i_{rd}}{\delta L_r} + \dfrac{u_{rq}}{\delta L_r} - \omega_r (l_m/L_s)\psi \end{cases}$$

in which $\delta = 1 - L_m{}^2/(L_r L_s)$ is the penetration coefficient, and $\omega_r$is the rotor's electric speed in the same-pitch reference form.

In order to perform a separate control, and achieve an efficient performance, two different offset voltages are added to the dq voltage, as shown in fig. 3. The offset voltage can be calculated by:

(9)

$$\begin{cases} \Delta u_{rd} = -\omega_r \delta L_r i_{rq} \\ \Delta u_{rq} = \omega_r \delta L_r i_{rd} + \omega_r \left(\dfrac{L_m}{L_s}\right)\psi \end{cases}$$

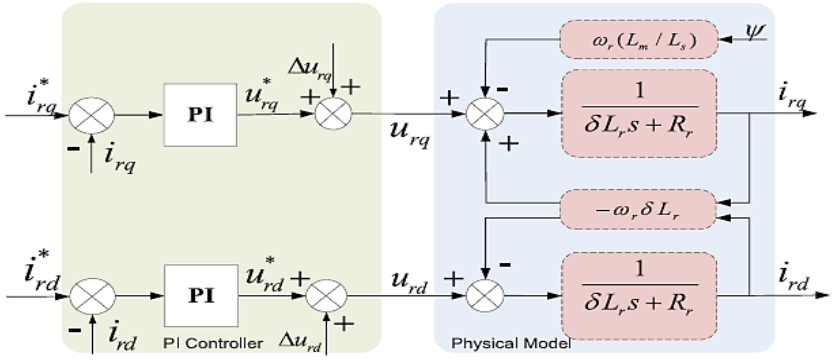

Figure 3. DFIG Model in dqCoordinate System (Hu et al., 2010)

In fact, the performance of a PI controller designed using this method depends on its change according to the system's parameter whose values should be determined in advance. Moreover, measured noise, flux saturation, and other nonlinear factors can lead to an increase in the power and size of the occurred error.

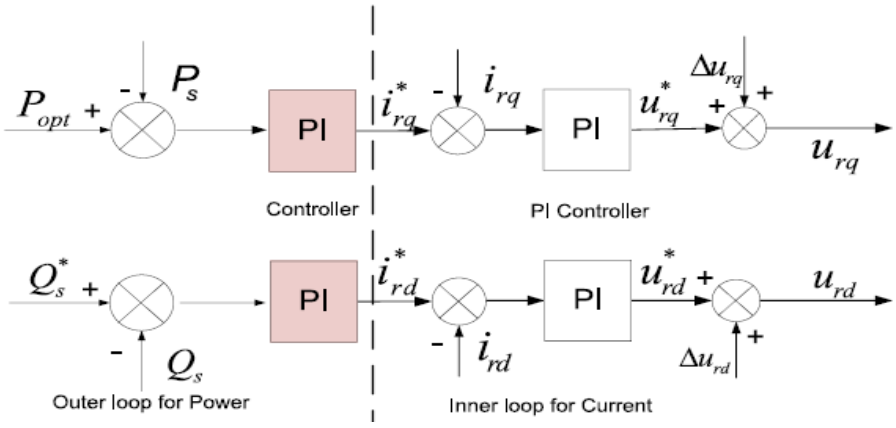

Figure 4. Two Control Modes for DFIG (Wu et al., 2018)

In fig. 4. The structure of active and reactive power is shown. The main purpose of the external circle is to adjust the active and reactive power. The external circle's output is considered as a reference for the internal circle.

The Dynamic Behavior of DFIG in the Stator's Static Reference Frame

The momentary active and reactive power outputs of the stator, moving from the DFIG to the grid can be calculated by:

(10)

$$P_s + jQ_s = -1.5U^s_{s\alpha\beta} \times \hat{I}^s_{s\alpha\beta}$$

And

(11)

$$P_s = -1.5\,(u_{s\alpha}i_{s\alpha} + u_{s\beta}i_{s\beta})$$

And

(12)

$$Q_s = -1.5\,(u_{s\beta}i_{s\alpha} - u_{s\alpha}i_{s\beta})$$

In the above relations $P_s>0$ and $P_s<0$ mean that DFIG acts as a generator, and a motor respectively. $Q_s>0$ and $Q_s<0$ indicate that DFIG imports the capacitive and inductive reactive power to the grid respectively.
Furthermore, the electromagnetic torque can be expressed by the following equation:

(13)

$$T_e = \frac{3}{2}\frac{pL_m Im(\psi^s_{s\alpha\beta} \times \hat{\psi}^s_{r\alpha\beta})}{(\sigma L_s L_r)}$$

In the above equation, p is the number of pairs of poles. Consequently, the mechanical-electrical equation of a DFIG system guided by a wind turbine can be expressed by:

$$\frac{J}{p}\frac{d\omega_r}{dt} = T_m - T_e \quad (14)$$

Momentary changes in the stator's current with α and componentscan be expressed as:

(15)

$$\frac{di_{s\alpha}}{dt} = \frac{1}{\sigma L_m}\left[u_{r\alpha} - R_r i_{r\alpha} - \frac{L_r}{L_m}(u_{s\alpha} - R_s i_{s\alpha})\right] - \frac{\omega_r}{\sigma L_m}\left(\sigma L_m i_{s\beta} + \frac{L_r}{L_m}\psi_{s\beta}\right)$$
$$\frac{di_{s\beta}}{dt} = \frac{1}{\sigma L_m}\left[u_{r\alpha} - R_r i_{r\beta} - \frac{L_r}{L_m}(u_{s\beta} - R_s i_{s\beta})\right] + \frac{\omega_r}{\sigma L_m}\left(\sigma L_m i_{s\alpha} + \frac{L_r}{L_m}\psi_{s\alpha}\right)$$

By substituting equations (12) and (13) into equation (12) and arranging them in a matrix form we have:

(16)

$$\frac{d}{dt}\begin{bmatrix}P_s\\Q_s\end{bmatrix} = -\frac{3}{2}\frac{1}{\sigma L_m}\begin{bmatrix}u_{s\alpha} & u_{s\beta}\\u_{s\beta} & -u_{s\alpha}\end{bmatrix}\begin{bmatrix}u_{r\alpha}\\u_{r\beta}\end{bmatrix} - \frac{3}{2}\frac{\omega_r L_r}{\sigma L_m^2}\begin{bmatrix}u_{s\beta} & -u_{s\alpha}\\-u_{s\alpha} & -u_{s\beta}\end{bmatrix}\begin{bmatrix}\psi_{s\alpha}\\\psi_{s\beta}\end{bmatrix} - \frac{3}{2}\frac{R_r}{\sigma L_m}\begin{bmatrix}-u_{s\alpha} & -u_{s\beta}\\-u_{s\beta} & u_{s\alpha}\end{bmatrix}\begin{bmatrix}i_{r\alpha}\\i_{r\beta}\end{bmatrix}$$
$$+\begin{bmatrix}\frac{L_r}{\sigma L_m^2}R_s & -\omega_{slip}\\ \omega_{slip} & \frac{L_r}{\sigma L_m^2}R_s\end{bmatrix}\begin{bmatrix}P_s\\Q_s\end{bmatrix} + \frac{3}{2}\frac{L_r}{\sigma L_m^2}\begin{bmatrix}u_{s\alpha}^2 + u_{s\beta}^2\\0\end{bmatrix}$$

In the above equation $\omega_{slip} = \omega_1 - \omega_r$ is the angular frequency of slip.

Results of the Simulation

Figure 5 shows the block diagram of the implemented system. The parameters of the DFIG system studied in this paper are brought in Table 1. In addition, the dc converter connection voltage was set at 120 watts. In the course of the simulations, a 4 kHz sampling frequency was selected for the suggested control strategy. Due to the use of asymmetrical SVM technique, the converter's switching frequency was set at 1 kHz.

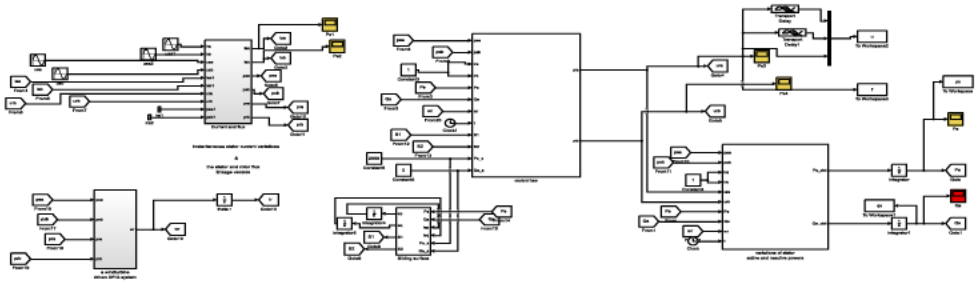

Figure 5. Block diagram of the studied system (Sitharthan et al., 2018)

A high frequency ac filter is connected to the stator for absorbing the switching harmonics generated by the two converters.

Table 1. Parameters of the DFIG simulated system

The evaluated power	2.0 MW
Line to line voltage	690 V
Stator frequency	50 Hz
Stator to rotor ratio	3
Rs (ohm)	0.001518
Rr (ohm) (related to the stator)	0.002087
Lσs (mH)	0.059906
Lσr(mH) (related to the stator)	0.082060
Lm (mH)	2.4
Pairs of poles	2
Inertia constant (kg.m^2)	17.23

The voltages and currents are sampled in the beginning of each sampling period. Then, the rotor control voltage needed for the sampling period is measured and transferred to SVM module.

In order to study the performance of the suggested strategy of direct control of the active and reactive power based on the sliding mode approach, the PI parameters related to the VC current controller are set at 0.12 and 0.005 respectively. For a direct control of the active and reactive power, the sampling time is set at 20 kHz, and the bandwidth of hysteresis controllers of the active and reactive power is determined at ±2 percent of the evaluated 2 megawatts power of the generator. The SMC control parameters for the suggested direct controlling of the active and reactive power is shown in Table 2.

Table 2. The regulating parameters of the SMC controller

Positive values of kp and kq	3500
Control values of kp1 and kq1	35000
Width of boundary layers λ1, λ2	200000, 250000

Figure 6 shows the three-phase current's wave. Moreover, the shape of the current's wave when the active power input is stepped is shown in Figure 7.

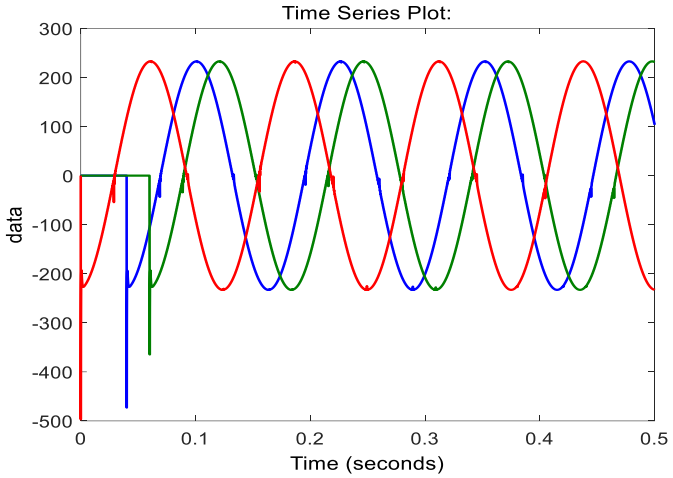

Figure 6. Waveform of the three-phase current

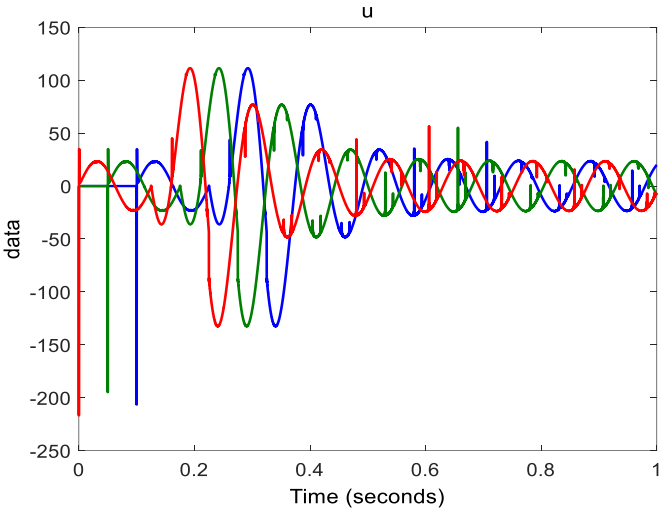

Figure 7. Waveform of the current when the active power input is stepped

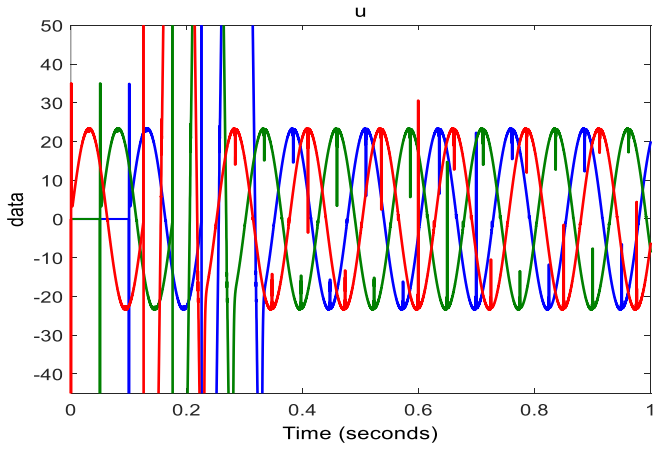

Figure 8. Waveform of the current in presence of an indeterminacy and the active power change

By performing the simulation, Ps and Qs that are the grid's active and reactive powers respectively can be obtained as Figures 9 and 10.

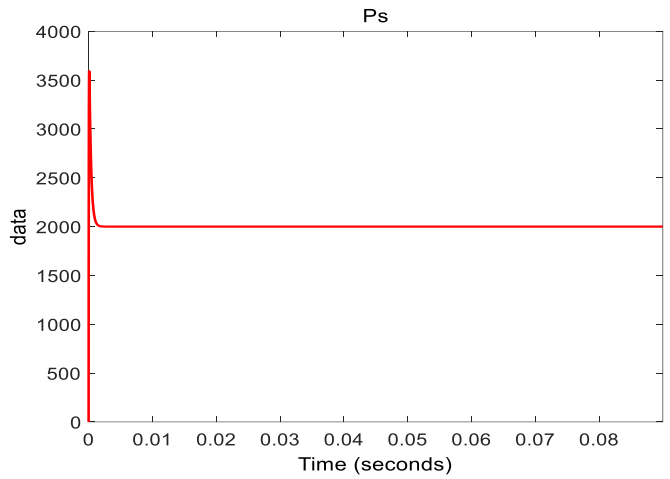

Figure 9. Waveform of the active power in tracking the reference power 2000 (2MW)

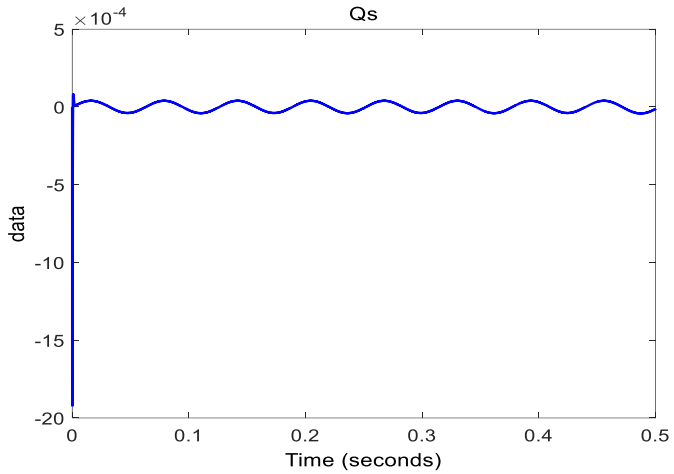

Figure 10. Waveform of the reactive power (that should be zero)

As indicated in Figures 9 and 10, using the suggested strategy, the active power is fairly successful in following the reference power. Furthermore, the reactive power has reached the range of zero with a tolerance of ±0.01 % that indicates the high performance of the suggested method.

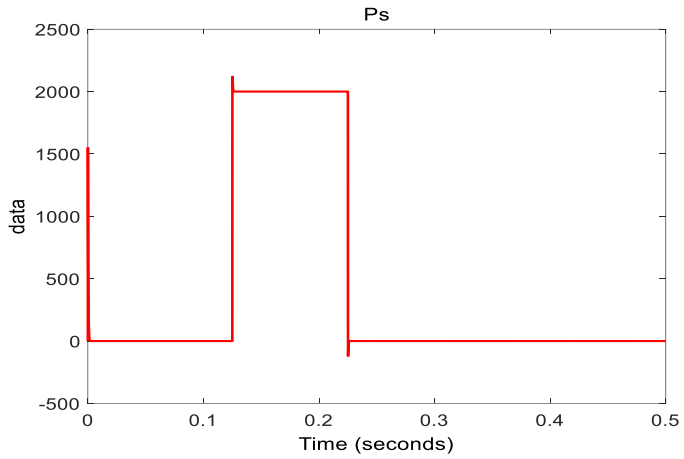

Figure 11. Waveform of the active power in tracking the power as a step function

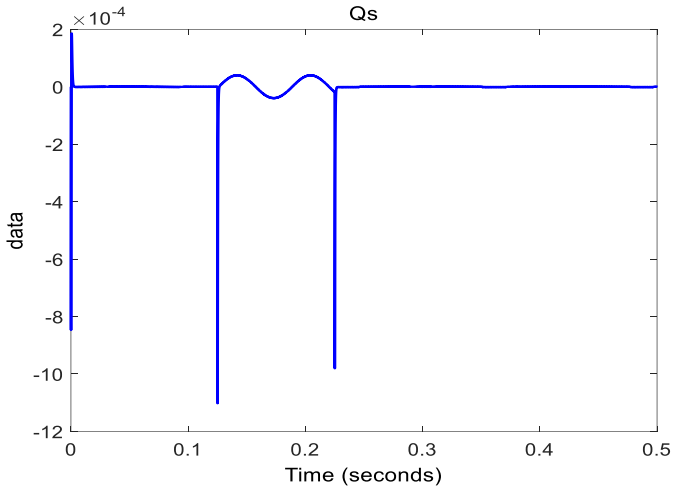

Figure 12. Waveform of the reactive power in a reference input of zero relative to the step's active power

As indicated in Figures 11 and 12, the active power has moved from 0.125 seconds with a very low error rate (approximately zero) and returns to zero at 0.225 seconds. This implies the highly efficient performance of the suggested method.

Optimizing the Performance of SMC Controller by Changing the Slip Function

Due to the fact that*sgn* function is used as the switching function for chattering reduction, one can still optimize this function through a series of changes, and reduce the sliding mode control chattering. Based on the abovementioned issues, a comparison is done between the controllers' performance in tracking the active and reactive power in 3 modes of using the sliding mode controller with $sgn\left(S_j\right)$, $tanh\left(S_j\right)$, and $sat\left(S_j\right)$ functions.

First Scenario: 2000 Watts (2MW) Active Power

In the first scenario, performance of the sliding mode controller, with the suggested slip functions, in tracking a 2000 watts' active power imported by the DFIG to the grid is studied.

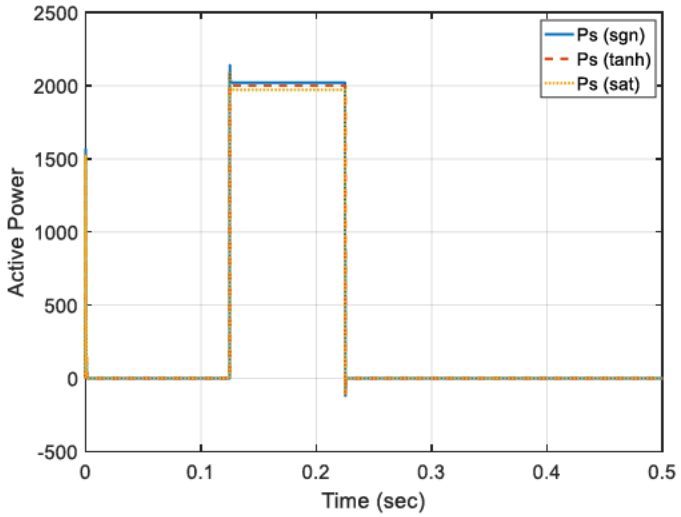

Figure 13. Comparing the impact of changing the SMC controller's slip function in tracking the active power of the step

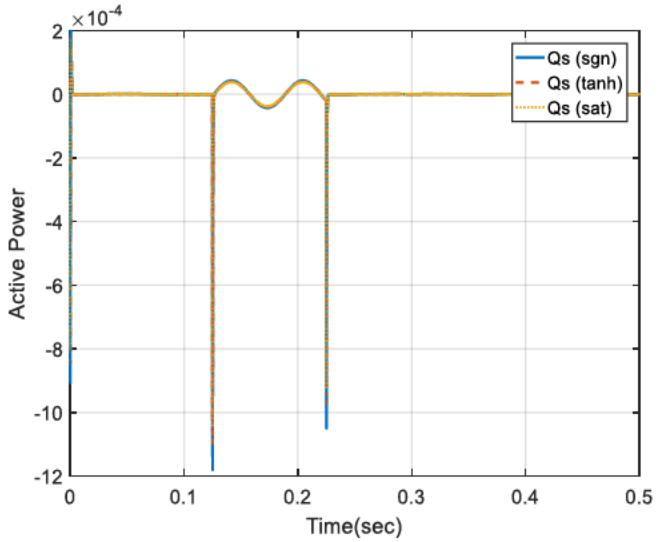

Figure 14. Comparing the impact of changing the SMC controller's slip function in zero reference input relative to the active power of the step

It is possible to observe the extent to which the control system is changed and optimized in Figures 13 and 14. The optimization takes place due to the reduction and elimination of chattering, caused by using $sat\ (S_j)$and $tanh\ (S_j)$functions, instead of $sgn\ (S_j)$. By optimizing the controlling function, one can look forward to the practicality of this research, and also the reliability of the control system in using it for control issues with larger powers.

Second Scenario: 500 Watts (500 W) Active Power

In the second scenario, performance of the sliding mode controller, with the suggested slip functions, in tracking a 500 watts' active power imported by the DFIG to the grid is studied.

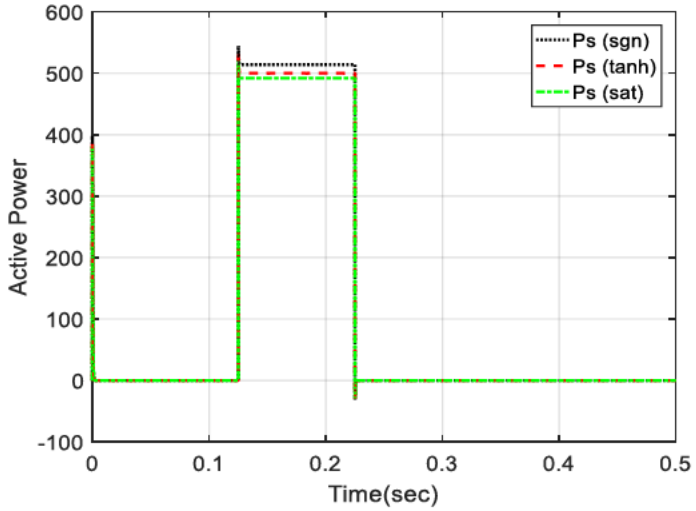

Figure 15. Comparing the impact of changing the SMC controller's slip function in tracking the active power of the step

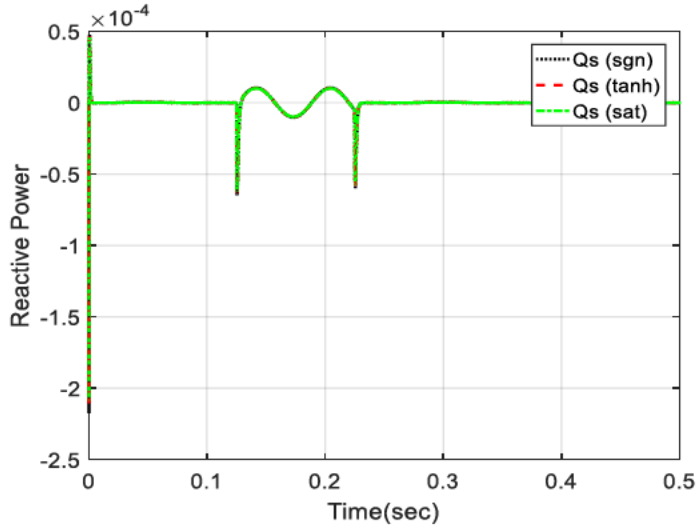

Figure 16. Waveform of the reactive power. Comparing the impact of changing the SMC controller's slip functionin zero reference input relative to the active power of the step

According to Figures 15 and 16, it can be seen that similar to the first scenario, using $sat\ (S_j)$and $tanh\ (S_j)$ functions instead of $sgn\ (S_j)$leads to a more precise and optimized performance of the controller.

Third Scenario: 4000 Watts (4 MW) Active Power

In the third scenario, performance of the sliding mode controller, with the suggested slip functions, in tracking a 4000 watts' active power imported by the DFIG to the grid is studied.

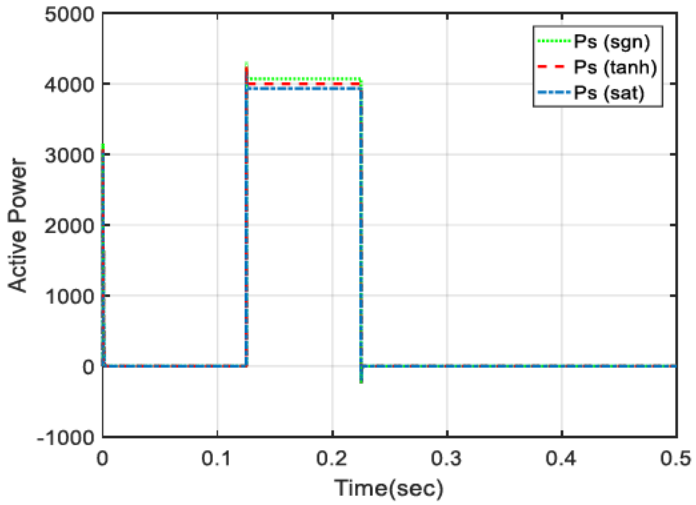

Figure 17. Comparing the impact of changing the SMC controller's slip function in tracking the active power of the step

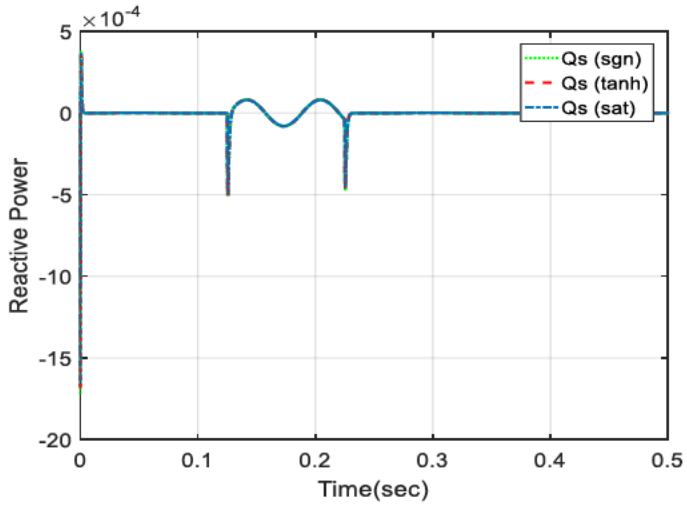

Figure 18. Waveform of the reactive power. Comparing the impact of changing the SMC controller's slip function in zero reference input relative to the active power of the step

Similar to the first two scenarios, and based on Figures 17 and 18, the rate of change and optimization of the control system can be seen. The optimization is caused by the reduction and elimination of chattering due to the use of $sat\ (S_j)$and $tanh\ (S_j)$functions instead of $sgn\ (S_j)$. In what follows, a comparison is made between the rates of error in tracking active and reactive power by the three scenarios with conventional and proposed functions. The results are shown in Table 3.

Table 3. Comparing the steady state error in tracking active and reactive power by the SMC controller with the suggested slip functions in the three studied scenarios

Scenario	Slip function	Error in tracking active power	Error in tracking reactive power
First scenario 2000 W	$sgn\ (S_j)$	2.170E-02	2.263-02
	$tanh\ (S_j)$	1.012E-06	1.251e-05
	$sat\ (S_j)$	2.139E-02	2.158-02
Second scenario	$sgn\ (S_j)$	1.009	1.033

500 W	$tanh\left(S_j\right)$	1.283E-05	1.592E-05
	$sat\left(S_j\right)$	2.942E-02	3.530E-02
Third scenario 4000 W	$sgn\left(S_j\right)$	5.236E-02	6.754E-02
	$tanh\left(S_j\right)$	1.826E-06	2.501E-06
	$sat\left(S_j\right)$	2.482E-02	4.258E-02

According to Table 3, it can be seen that with changing the slip function, the performance of the sliding mode controller in tracking active and reactive power is optimized. The optimization is not only manifest in the controlling function, but also evident in the system's rate of steady state error.

Conclusion

This article attempted at modelling and studying the doubly-fed induction generator (DFIG). Furthermore, a review of one of the most significant controlling methods of complex systems, called sliding mode control, is done. Then, the design of a practical and direct controlling of active and reactive power for a grid-connected DFIG system was proposed based on the sliding mode control approach. The investigations and simulations were done using MATLAB software. Designing the controller with an adequate controlling law was done mathematically for a DFIG system connected to a 2 MW grid. The results of the simulation indicated a desirable performance of the proposed method. In this paper, two optimizations were provided for the performance of the SMC control system through changing the slip function, and the efficiency of the method was studied in the three 2000 W, 500 W, and 4000 W scenarios. Moreover, it was shown that a better and more accurate performance of the control system is obtainable.

References

1. Bartolini, G., Pisano, A., Punta, E. and Usai, E., 2003. A survey of applications of second-order sliding mode control to mechanical systems. International Journal of control, 76(9-10), pp.875-892.
2. Bekka, H., Taraft, S., Rekioua, D. and Bacha, S., 2013. Power Control Of A Wind Generator Connected To The Grid In Front Of Strong Winds. Journal of Electrical Systems, 9(3).
3. Bektache, A. and Boukhezzar, B., 2018. Nonlinear predictive control of a DFIG-based wind turbine for power capture optimization. International Journal of Electrical Power & Energy Systems, 101, pp.92-102.
4. Bianchi, F.D., De Battista, H. and Mantz, R.J., 2010. Robust Multivariable Gain-Scheduled Control of Wind Turbines for Variable Power Production. International journal of systems control, 1(3).
5. Boukhezzar, B., Lupu, L., Siguerdidjane, H. and Hand, M., 2007. Multivariable control strategy for variable speed, variable pitch wind turbines. Renewable Energy, 32(8), pp.1273-1287.
6. Duong, M.Q., Leva, S., Mussetta, M. and Le, K.H., 2018. A Comparative Study on Controllers for Improving Transient Stability of DFIG Wind Turbines During Large Disturbances. Energies, 11(3), p.480.
7. Femia. N, Fortunato. M, "Dynamic model of one-cycle control for converters operating in continuous and discontinuous conduction modes", in International Journal of Circuit Theory and Applications, Vol. 37.No.5, pp.661–686,2009.
8. Hu, J., Nian, H., Hu, B., He, Y. and Zhu, Z.Q., 2010. Direct active and reactive power regulation of DFIG using sliding-mode control approach. IEEE Transactions on energy conversion, 25(4), pp.1028-1039.
9. Munje, R., Patre, B. and Tiwari, A., 2018. Sliding Mode Control. In Investigation of Spatial Control Strategies with Application to Advanced Heavy Water Reactor (pp. 79-91). Springer, Singapore.

10. Ramadge, P.J. and Wonham, W.M., 1987. Supervisory control of a class of discrete event processes. SIAM journal on control and optimization, 25(1), pp.206-230.
11. Rocha-Osorio, C.M., Solís-Chaves, J.S., Golestan, S., Costa, F.F., Fernandes, D.A., Guerrero, J.M. and Sguarezi Filho, A.J., 2018. Morphological PLL for potential applications on renewable energy. Electric Power Systems Research, 156, pp.15-23.
12. Shtessel, Y., Edwards, C., Fridman, L. and Levant, A., 2014. Conventional sliding mode observers. In Sliding Mode Control and Observation (pp. 105-141). Birkhäuser, New York, NY.
13. Sitharthan, R., Sundarabalan, C.K., Devabalaji, K.R., Nataraj, S.K. and Karthikeyan, M., 2018. Improved fault ride through capability of DFIG-wind turbines using customized dynamic voltage restorer. Sustainable Cities and Society, 39, pp.114-125.
14. Wu, L., Mazumder, S.K. and Kaynak, O., 2018. Sliding Mode Control and Observation for Complex Industrial Systems—Part II. IEEE Transactions on Industrial Electronics, 65(1), pp.830-833.
15. Yanhua. L, Zhang. Xu, Zhao, Dongmei. M, "Research on the Wind Farm Reactive Power Compensation Capacity and Control Target", in Asia Pacific Power and Energy Engineering Conference (APPEEC), pp.1-5, 2011.
16. Yu, H., 2017. A critical review on the simulations of wind turbine aerodynamics focusing on hybrid RANS-LES methods. Energy, 138, pp.257-289.
17. Zuo, H., Bi, K. and Hao, H., 2018. Dynamic analyses of operating offshore wind turbines including soil-structure interaction. Engineering Structures, 157, pp.42-62.